PCCP

PAPER

View Article Online
View Journal

Cite this: DOI: 10.1039/d5cp02133b

Spatially controlled plasmon-induced photopolymerization at the apex of gold nanobipyramids: paving the way for 3D nanofabrication†

Amine Khitous, [ab] Céline Molinaro, [ab] Loic Vidal,[ab] Stephania Abdallah,[ab] Anthony Désert, [c] Frédéric Lerouge, [c] Jean-Pierre Malval, [ab] Stephane Parola [c] and Olivier Soppera *[ab]

Received 6th June 2025,
Accepted 15th July 2025

DOI: 10.1039/d5cp02133b

rsc.li/pccp

In this study, we investigate near-field photopolymerization at the tips of gold nanobipyramids (AuNBPs) under linearly polarized irradiation conditions with femtosecond pulses in the near infrared region. TEM was used to visualize the localisation and spatial extend of the polymer resulting from the near-field photopolymerization. The single-tilt mode in TEM provides 3D information of the position of the nanoparticle on the substrate and the polymer lobes. In particular, we demonstrate that photopolymerization is localized mainly at the tips of AuNBPs, in line with the electromagnetic field distribution expected by simulations. We observed experimentally that when AuNBPs lie on the substrate *via* a facet, asymmetrical polymerization occurred: while polymerization is constrained by the substrate on the side in contact with the surface, we showed the possibility of fabricating a nano-sized polymer volume in 3D *via* near-field photopolymerization. These results illustrate the great control of photopolymerization at the nanoscale and represent a major step towards 3D fabrication at nanometer resolution.

Introduction

It is well established that the distribution and intensity of the electric field around metallic nanoparticles (MNPs) under irradiation depend strongly on the dielectric properties of the surrounding medium, as well as on the size, shape and orientation of the nanoparticle.[1–6] These parameters, represented by the aspect ratio, directly influence the position of the localized surface plasmon resonance (LSPR) bands and the extinction values.[7,8] Understanding the distribution and intensity of the electric field is crucial for optimizing applications such as sensing,[9–11] photocatalysis[12–14] or photonics.[15–17]

One of the specific features of gold bipyramidal nanoparticles (AuNBPs) compared with other nanoobjects (nanospheres, nanorods, plates, nanocubes, *etc.*) is that two distinct possible orientations are observed when deposited on a substrate: either in contact along a facet or with its principal longitudinal axis parallel to the substrate. The optical properties of AuNBPs then depend on their configuration. For example, the orientation of AuNBPs has a direct influence on the surface enhanced Raman spectroscopy (SERS) signal.[8] Furthermore, recent works have revealed the appearance of multipolar modes of plasmon resonance depending on the orientation of the MNPs and their contact with the substrate, thus increasing light enhancement and sensitivity to refractive index variations.[7,18–21]

In this study, we investigate the near-field photoinduced polymerization under 800 nm excitation around AuNBPs (Fig. 1). The near-field photoinduced polymerization (NFPP) method has aroused interest for exploration of LSPR phenomena *via* reactions that are photosensitive to light.[1,22–24] Our recent work has revealed that the polymerization is more efficient at angular ends of nanostructures, highlighting the importance of geometry in plasmonic interactions.[1] These studies have always been limited to 2D analyses, as the NPs are deposited on a substrate and the TEM-based observation mode offers a 2D projection.

In this study, we investigate the electric field distribution for AuNBPs deposited on a Si_3N_4 substrate, studying the orientation of isolated particles on the surface as well as the localization of NFPP on the AuNBP surface. This analysis is carried out using transmission electron microscopy (TEM) in single-tilt mode, in order to precisely visualize the polymer distribution around the AuNBPs in 3D. These experimental results are compared with simulations of spectra and intensity maps

[a] *Université de Haute Alsace, CNRS, IS2M UMR 7361, F-68100 Mulhouse, France. E-mail: olivier.soppera@uha.fr*
[b] *Université de Strasbourg, France*
[c] *Ecole Normale Supérieure de Lyon, CNRS, Université Lyon 1, Laboratoire de Chimie UMR 5182, 46, allée d'Italie, F69364, Lyon Cedex 07, France*

† Electronic supplementary information (ESI) available. See DOI: https://doi.org/10.1039/d5cp02133b

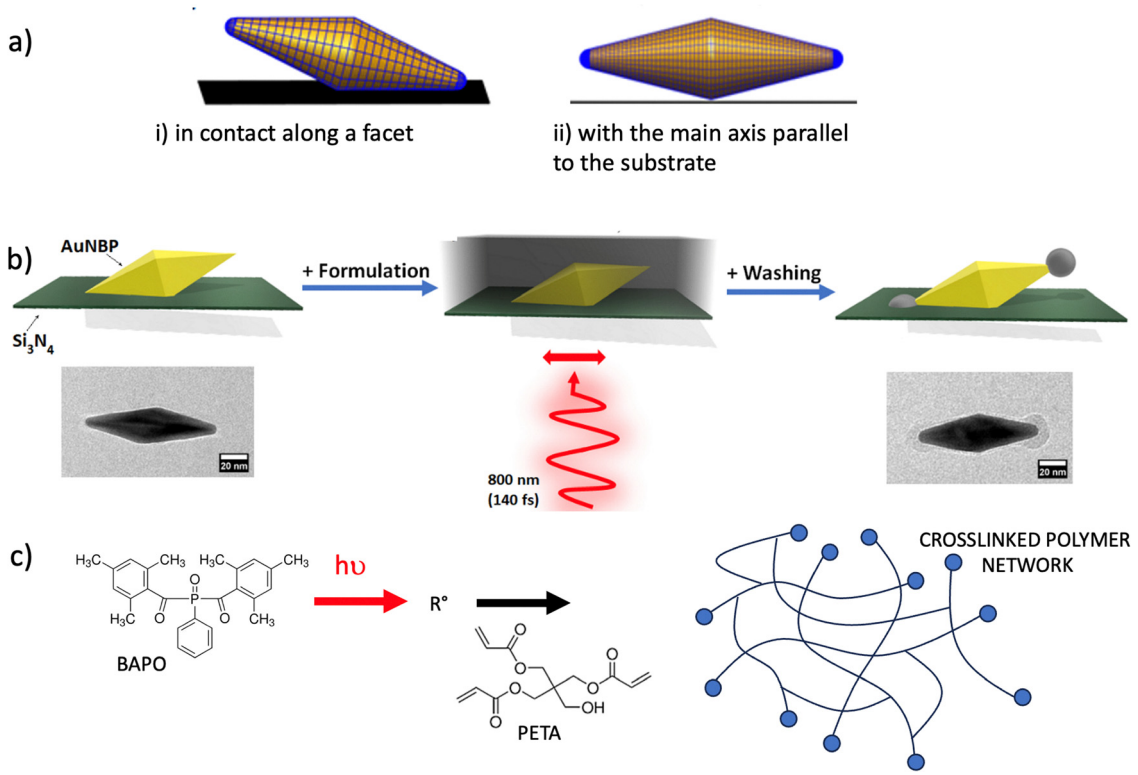

Fig. 1 (a) The possible orientations of AuNBPs on the substrate surface (i) in contact along a facet or (ii) with the main axis of the AuNBP parallel to the substrate. (b) Scheme illustrating the AuNBP irradiation method and TEM imaging. (c) Schematic of the polymerization process.

obtained through the Metallic NanoParticles Boundary Element Method (MNPBEM).[25,26]

Experimental section

Synthesis of AuNBPs

The AuNBPs used in this study were synthesized *via* a colloidal route following a previously reported procedure.[27] This method produces particles that are monodisperse, with target dimensions of 94 nm ± 6 nm in length, 29 nm ± 3 nm in width at the particle center, with a curvature radius at each tip of 5 nm.

Deposition of AuNBPs

To ensure the study was performed on single particles and avoid coupling effects, AuNBPs were deposited from dilute solutions onto TEM grids. TEM observation is performed at the level of 1500 μm × 100 μm rectangular windows of 50 nm-thick Si_3N_4 membranes (Ted Pella). The surfactant present in the colloidal solutions was removed by dilution and centrifugation. Next, AuNBPs deposited on the TEM grid were subjected to UV/ozone treatment for 2 hours (ProCleaner Plus UV, Bioforce) to remove surfactant residues, followed by rinsing with water. After this procedure, no surfactant layer was observable *via* TEM imaging (ARM200F JEOL).

Formulation and irradiation of AuNBPs

The photopolymerizable formulation used in this study (named F_{BAPO}) includes a photoinitiator, bis(2,4,6-trimethylbenzoyl) phosphine oxide (BAPO) from Sigma-Aldrich, and the monomer pentaerythritol triacrylate (PETA), used in previous studies.[1] The BAPO concentration was 1.5 wt%. BAPO exhibits single-photon absorption between 360 and 400 nm, but in our experiments, it is used as a two-photon photoinitiator at 800 nm using a Ti:sapphire laser (Chameleon Ultra II, Coherent), emitting 140 fs femtosecond pulses at a repetition rate of 80 MHz. We called F_{PETA} the monomer PETA alone.

Once prepared, the TEM grids are placed on a glass slide and a drop of the photocurable formulation is applied (Fig. 1). This is then mounted on a 3D piezoelectric stage, enabling the sample to be moved to the laser focal point. Irradiation parameters, such as laser power and exposure time, are computer-controlled. A Zeiss Axio Observer D1 inverted microscope, equipped with a high numerical aperture objective (NA 0.95, ×40), focuses the laser beam to obtain a spot 1.2 ± 0.3 μm in diameter at 800 nm. The samples are moved using the piezo stage under the linearly polarized beam at a speed of 10 μm s^{-1}, exposing each spot for 100 ms. Laser power is adjusted using an acousto-optic modulator.

Determining the photopolymerization threshold dose (D_t)

The photopolymerization threshold dose (D_t) corresponds to the minimum energy required to initiate the polymerization reaction at the focal point under far-field conditions. It was determined by irradiating the formulation with line patterns on the TEM grid without the presence of nanoparticles, modulating the incident power to determine the threshold time (t_T) at a

given fluence (expressed in mW cm^{-2}). In our study, D_t was measured at 18 kJ cm^{-2}. Subsequent experiments were conducted with doses between 8.5% and 26.5% of this threshold value to eliminate any far-field-induced polymerization reaction. The formulation without the photoinitiator does not polymerize for D_t, with and without nanoparticles, which confirms that the mechanism is photochemical. The threshold can be visualized by the change in the refractive index due to polymerization.

Experimental procedure and observation

After D_t determination, TEM grids with AuNBPs were irradiated at doses below the threshold dose, depending on the percentage of D_t applied. After irradiation, the grids were immersed in an acetone and ethanol bath to remove the unpolymerized formulation, before being carefully dried for observation. TEM images for each condition were acquired, and for each situation, at least five particles were analyzed. A representative image is provided.

Numerical simulations

Simulations of absorption, scattering and extinction cross-sections, as well as electric field maps, were carried out using the Metallic NanoParticle Boundary Element Method (MNPBEM)[25,26] in MATLAB. The AuNBPs were modeled as a bicone with a hemispherical tip. The dimensions of the simulated AuNBPs were 94 nm in length and 29 nm in diameter with a radius of curvature of 5 nm for the tips, corresponding to the dimensions determined using TEM. The refractive index of Au is taken from the study by Johnson and Christy,[28] and the refractive index of the surrounding medium was set at 1.48 (refractive index of the photopolymerizable formulation). The particle is placed 1 nm from the Si_3N_4 substrate (mimicking the remaining CTAB layer between the NP and the substrate), whose refractive index is 2.02, and considered an infinite substrate. The AuNBP is illuminated from the substrate under normal incidence with linear polarization. The field maps have been generated with illumination at 800 nm wavelength. All maps show the squared modulus of the electric field. All simulations are carried out in retarded mode.

Results and discussion

The AuNBPs studied in this work are deposited on a TEM-grid Si_3N_4 substrate and surrounded by the F_{BAPO} formulation (Fig. 1). It is known that isolated AuNBPs can orient themselves on the substrate surface in two orientations: (i) in contact along

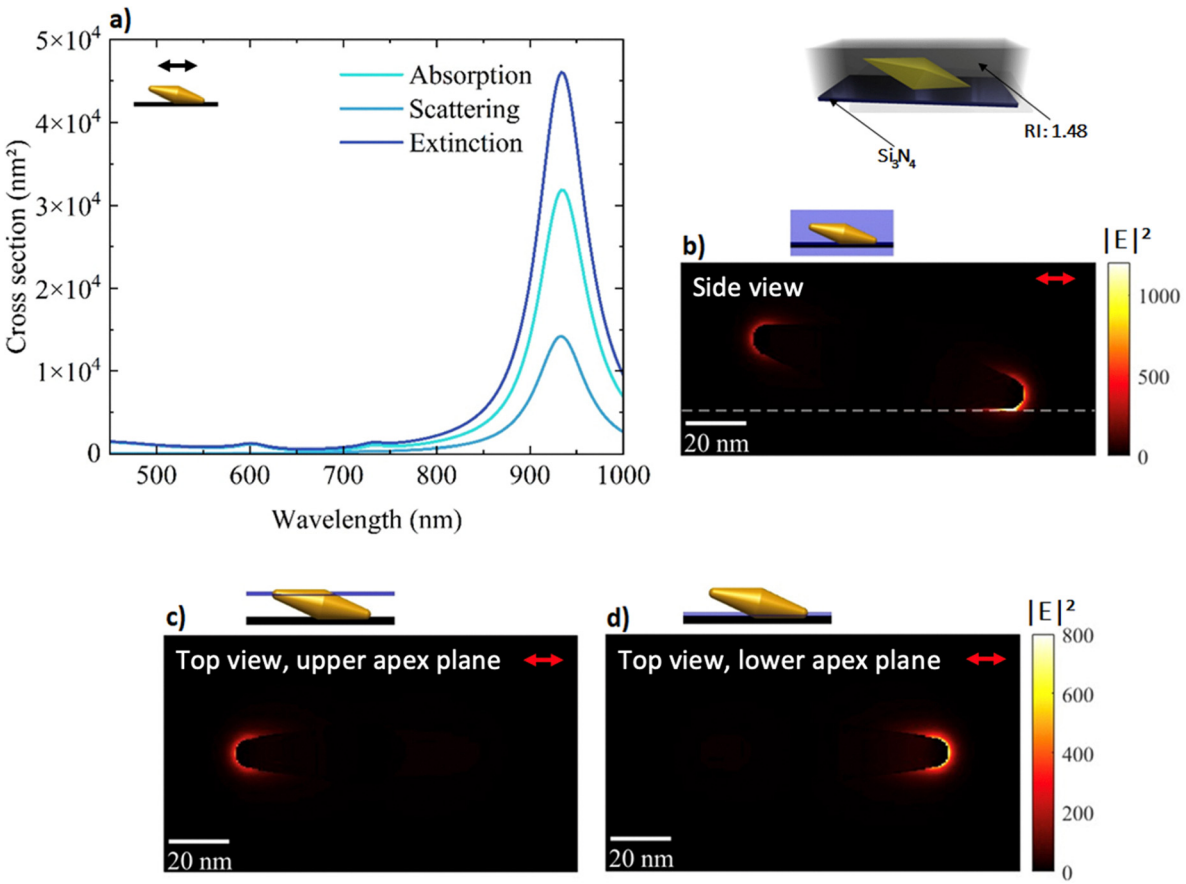

Fig. 2 Numerical simulation of the absorption, scattering and extinction cross section of an AuNBP deposited on a facet. (a) Intensity field map for illumination at 800 nm with a polarization along the AuNBP in the meridian plane through the tips (b), in the plane parallel to the substrate through the tip at the top (c) and through the tip at the bottom (d).

a facet or (ii) with the main axis of the AuNBP parallel to the substrate.[4,5]

We propose a method for determining the orientation of the AuNBPs on the substrate: a 12 nm gold film was deposited by evaporation on the AuNBPs previously deposited on the TEM grid. The AuNBPs create a shadow effect underneath them since the gold cannot be deposited under the AuNBPs. The surfaces are then imaged by TEM at different orientations in order to observe the area without gold. Fig. S1 (ESI†) shows a typical example. Two images of the sample in the same area are compared with angles (+30° −30°), and the shadow zone is shifted asymmetrically for the two apexes. This reveals a different distance from the substrate and confirms therefore that the AuNBPs are mainly deposited on one facet. The apex circled in red is suspended above the substrate. We observed that most NBPs were deposited in this configuration (i) in contact along a facet. We will therefore only consider this configuration in the following.

In order to describe the optical properties of the nanoparticles in this environment, simulations were carried out. Cross-section and intensity field distribution maps are presented in Fig. 2.

Simulations of the electric field intensity at 800 nm excitation with a linear polarization along with the axis of the AuNBPs show, as expected, that the field enhancement is mainly localized at the tips of the AuNBPs (Fig. 2b). It is interesting to note, however, that the tip in contact with the substrate has a larger field strength than that exposed only to the formulation (Fig. 2c and d). This difference of a factor of 1.8 is due to the difference in refractive indices between F_{BAPO} and Si_3N_4, with the latter having a higher refractive index. This result is consistent with studies by Vu *et al.*[29]

These simulation results of the electric field distribution are compared with the experimental results obtained by NFPP. A drop of formulation was deposited on the AuNBPs (Fig. 1) and irradiated at doses below the threshold dose for two-photon photopolymerization. As explained previously, these conditions do not allow photopolymerization to be initiated without the assistance of nanoparticles, particularly due to the presence of oxygen, which inhibits polymerization reactions. However, in the near field, the light is amplified by the AuNBPs, thus making it possible to exceed the threshold dose. As oxygen is consumed in this region, the polymerization reaction is initiated.[30,31] The study as a function of irradiation power is shown in Fig. 3.

The first line in Fig. 3 concerns the F_{BAPO} formulation (PETIA + BAPO 1.5 wt%). It can be seen that at powers less than or equal to 8.5% D_t, no polymerization reaction was observed. However, from 17.5% D_t, the NFPP reaction was initiated on the surface of AuNBPs. Polymer lobes are formed at the ends of the AuNBPs, which is consistent with the field maps shown in Fig. 2. At 26.5% D_t, an extension of the polymerized zone is observed, not only at the tips but also along the sides of the AuNBPs.

In order to demonstrate the photochemical nature of near-field polymerization, a control is performed using a drop of pure PETA (without the BAPO photoinitiator) deposited on the substrate and irradiated at the same doses as the F_{BAPO} formulation. TEM images show the absence of the polymer on the surface of AuNBPs at all three power levels tested, particularly at 17.5% D_t and 26.5% D_t. These results confirm the role of the photoinitiator (BAPO) in the near-field polymerization process. We confirm the photochemical nature of the polymerization observed in the case of F_{BAPO}.

Thermal polymerization could account for the formation of a thin polymer layer all around the nanoparticle surface. However, we do not think this explanation very plausible in our excitation conditions. Indeed, we verified that the thermal polymerization temperatures of PETA alone and PETA-BAPO were very close (determined by DSC: 216 °C for PETA and 208 °C for PETA-BAPO). The absence of the polymer with PETA alone

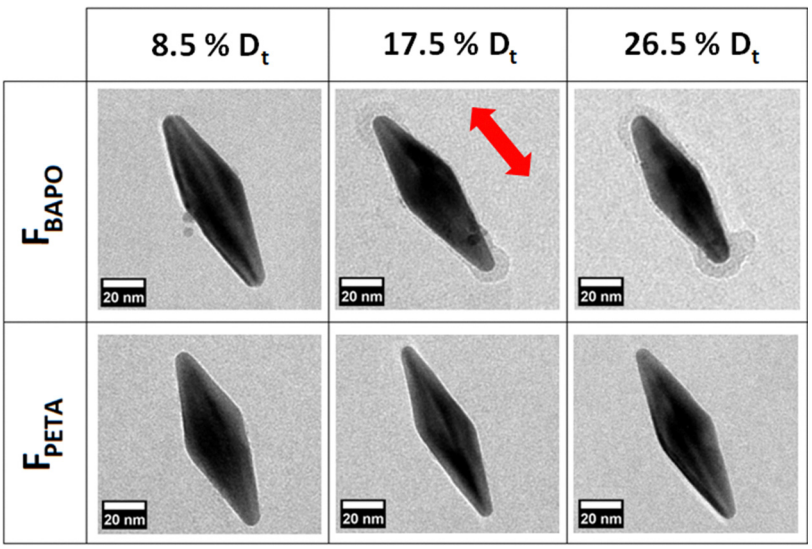

Fig. 3 Study of near-field photopolymerization as a function of power for F_{BAPO} and F_{PETA}. Excitation at 800 nm, and the red arrow shows the direction of polarization.

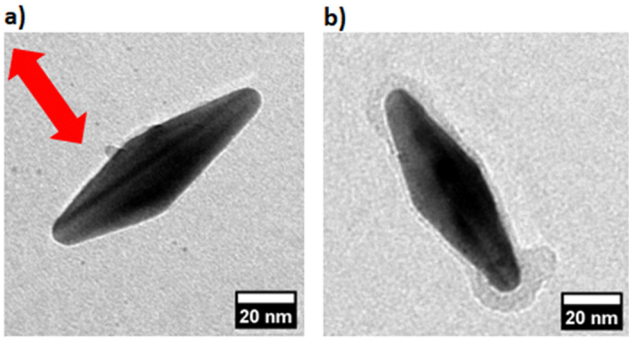

Fig. 4 Impact of polarization direction on NFPP (26.5% D_t) at 810 nm: (a) polarization along the transverse axis, (b) polarization along the longitudinal axis.

(at both the apex and the side of the NP) shows that the temperature increase is insufficient to initiate polymerization. A more plausible explanation we propose is linked to a local consumption of the inhibitor in the vicinity of the nanoparticles, which could locally lower the threshold dose for far-field polymerization. Near the nanoparticle surface, the enhanced near-field excitation leads to a more efficient activation of the photoinitiator compared to the far field. This results in a higher generation of radicals that consume the molecular oxygen acting as an inhibitor. Consequently, the inhibitor is more significantly depleted near the nanoparticle surface, triggering the onset of polymerization in this region. This result is consistent with the results obtained previously with short nanorods.[1]

Excitation of the dipolar modes of AuNBPs depends on the orientation of the AuNBPs with respect to the polarization direction of the light. The response of an AuNBP with its principal axis perpendicular to the direction of polarization is shown in Fig. 4. This result is compared with the previous one, using in both cases the same power for irradiation. TEM images reveal the ON/OFF behavior of the NFPP reaction as a function of light polarization. Specifically, when the polarization of the incident light is perpendicular to the long axis of the AuNBPs, no polymerization was observed, as the transverse mode of the AuNBPs is set at 520 nm and is much lower in intensity (Fig. S2, ESI†), making it impossible to reach the polymerization threshold by exciting at 800 nm.

Observation of TEM images of AuNBPs after photopolymerization reveals that the two polymer lobes are not symmetrical and show different contrasts (Fig. 3 and 4). A sharper contrast can be seen on one of the two tips, suggesting that the volume

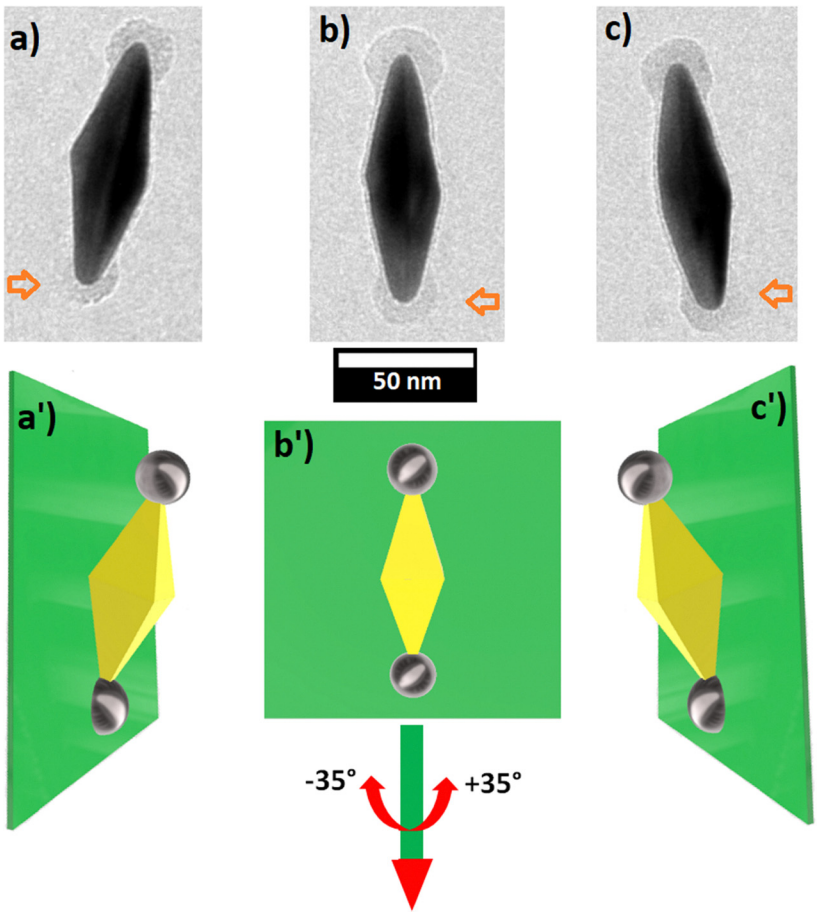

Fig. 5 Observation of polymer distribution around AuNBPs in TEM: (a) tilt −35°, (b) tilt 0° and (c) tilt −35°. (a′), (b′) and (c′) are schematic representations of images (a), (b) and (c), respectively.

of polymer is greater on one of the tips than on the other. Since the TEM images are shown in top view, tilt-mode TEM analyses were performed to visualize the orientation of the two polymer lobes on the two tips. The tilt-mode TEM images are shown in Fig. 5.

The TEM image in Fig. 5a shows that the two polymer lobes are well defined. However, a -35° rotation of the substrate (Fig. 5b) reveals that the polymer lobe on the AuNBP side loses contrast on its left half (see the orange arrows). Conversely, a $+35^\circ$ rotation shows that the right half of the same lobe exhibits reduced contrast. Notably, in both rotations, the lobe located on the raised vertex remains well defined with no loss of contrast.

The change in the appearance of this polymer lobe with angle is consistent with the schematic shown in Fig. 5, corresponding to a half hemisphere placed on the substrate at the end of the AuNBP. As explained previously, this side of the AuNBP corresponds to the greatest field exaltation, but the polymerized volume is limited by the presence of the substrate, which explains the formation of a half hemisphere in this area of space.

As for the other lobe, the observation is different: firstly, this lobe is better defined, with a sharper contrast that can be interpreted by a greater polymer thickness. The position and shape of this polymer lobe do not change as the angle changes, showing that the polymer lobe is indeed in suspension, attached to the end of the AuNBP and detached from the substrate.

The absence of polymerization under the particle demonstrates the very good spatial control of 3D polymerization. These results demonstrate that NBPs are excellent nano-object geometries for forming 3D-polymerized nanovolumes. Suspended lobes have a diameter of less than 20 nm, a resolution unprecedented for photopolymerized polymers. These results complement our previous study comparing the responses of a family of nanoobjects for which the contrast generated between hot spots and low-field parts were correlated with the resolution obtained in the near-field. Ultimately, we demonstrate that this plasmon-assisted polymerization concept can be applied to 3D nanofabrication on the scale of a few nanometers and is not limited to 2D substrate nanofabrication demonstrations. These results open up infinite prospects for 3D nanofabrication using this type of nanoobject.

Conclusions

In this study, we demonstrated the ability of gold nanobipyramids (AuNBPs) to induce localized near-field photopolymerization under femtosecond near-infrared irradiation. Transmission electron microscopy analysis confirmed that polymer growth occurs preferentially at the tips of AuNBPs, in agreement with numerical predictions of electromagnetic field intensification. In addition, we have highlighted a 3D light–matter interaction, where the volume of polymer formed is localized well at the end of the AuNBP, detached from the substrate. These results represent a significant step forward in the development of nanoscale additive manufacturing techniques, paving the way for new applications in nanophotonics, sensors and functional nanostructures.

Conflicts of interest

There are no conflicts to declare.

Data availability

The data supporting this article have been included in the main file and as part of the ESI.†

Acknowledgements

The authors acknowledge ANR for funding (POPCORN grant number ANR-21-CE09-0035) and PEPR LUMA Project Sunrise (Grant number ANR-23-EXLU-0003). This work of the Interdisciplinary Institute HiFunMat, as part of the ITI 2021–2028 program of the University of Strasbourg, CNRS and INSERM, was supported by IdEx Unistra (ANR-10-IDEX-0002) and SFRI (STRAT'US project, ANR-20-SFRI-0012) under the framework of the French Investments for the Future Program.

References

1 A. Khitous, C. Molinaro, S. Abdellah, S. Marguet, G. Laurent, L. Vidal, J.-P. Malval, C. Fiorini-Debuisschert5, P.-M. Adam, L. Douillard, R. Bachelot and O. Soppera, Spatial Distribution of the Photopolymerization Induced by Localized Surface Plasmons: Impact of the Morphology of the Au Nanoparticles, *J. Phys. Chem. C*, 2024, **128**(31), 13097–13107.

2 E. A. Coronado, E. R. Encina and F. D. Stefani, Optical Properties of Metallic Nanoparticles: Manipulating Light, Heat and Forces at the Nanoscale, *Nanoscale*, 2011, **3**(10), 4042–4059.

3 K. L. Kelly, E. Coronado, L. L. Zhao and G. C. Schatz, The Optical Properties of Metal Nanoparticles: The Influence of Size, Shape, and Dielectric Environment, *J. Phys. Chem. B*, 2003, **107**, 668–677.

4 Y. M. Morozov, N. Gisbert Quilis, S. Fossati, L. De Laporte, C. Gusenbauer, A. Weber, J. L. Toca-Herrera, F. Wiesner, U. Jonas and J. Dostalek, Plasmon-Enhanced Multiphoton Polymer Crosslinking for Selective Modification of Plasmonic Hotspots, *J. Phys. Chem. C*, 2024, **128**(43), 18641–18650, DOI: **10.1021/acs.jpcc.4c05936**.

5 A. Sundaramurthy, P. J. Schuck, N. R. Conley, D. P. Fromm, G. S. Kino and W. E. Moerner, Toward Nanometer-Scale Optical Photolithography: Utilizing the Near-Field of Bowtie Optical Nanoantennas, *Nano Lett.*, 2006, **6**(3), 355–360, DOI: **10.1021/nl052322c**.

6 S. Nah, L. Li, R. Liu, J. Hao, S. B. Lee and J. T. Fourkas, Metal-Enhanced Multiphoton Absorption Polymerization

with Gold Nanowires, *J. Phys. Chem. C*, 2010, **114**(17), 7774–7779, DOI: 10.1021/jp100387k.

7 H. Chen, L. Shao, T. Ming, K. C. Woo, Y. C. Man, J. Wang and H.-Q. Lin, Observation of the Fano Resonance in Gold Nanorods Supported on High-Dielectric-Constant Substrates, *ACS Nano*, 2011, **5**(8), 6754–6763, DOI: 10.1021/nn202317b.

8 Q. Shi, K. J. Si, D. Sikdar, L. W. Yap, M. Premaratne and W. Cheng, Two-Dimensional Bipyramid Plasmonic Nanoparticle Liquid Crystalline Superstructure with Four Distinct Orientational Packing Orders, *ACS Nano*, 2016, **10**(1), 967–976, DOI: 10.1021/acsnano.5b06206.

9 C. Fang, G. Zhao, Y. Xiao, J. Zhao, Z. Zhang and B. Geng, Facile Growth of High-Yield Gold Nanobipyramids Induced by Chloroplatinic Acid for High Refractive Index Sensing Properties, *Sci. Rep.*, 2016, **6**(1), 36706.

10 A. Khitous, C. Molinaro, S. Gree, K. Haupt and O. Soppera, Plasmon-Induced Photopolymerization of Molecularly Imprinted Polymers for Nanosensor Applications, *Adv. Mater. Interfaces*, 2023, **10**(7), 2201651.

11 Y. Zhang, J. Jiao, Y. Wei, D. Wang, C. Yang and Z. Xu, Plasmonic Colorimetric Biosensor for Sensitive Exosome Detection via Enzyme-Induced Etching of Gold Nanobipyramid@MnO_2 Nanosheet Nanostructures, *Anal. Chem.*, 2020, **92**(22), 15244–15252, DOI: 10.1021/acs.analchem.0c04136.

12 A. Khitous, L. Noel, C. Molinaro, L. Vidal, S. Grée and O. Soppera, Sol–Gel TiO_2 Thin Film on Au Nanoparticles for Heterogeneous Plasmonic Photocatalysis, *ACS Appl. Mater. Interfaces*, 2024, **16**(8), 10856–10866, DOI: 10.1021/acsami.3c15866.

13 Z. Bian, T. Tachikawa, P. Zhang, M. Fujitsuka and T. Majima, Au/TiO_2 Superstructure-Based Plasmonic Photocatalysts Exhibiting Efficient Charge Separation and Unprecedented Activity, *J. Am. Chem. Soc.*, 2014, **136**(1), 458–465, DOI: 10.1021/ja410994f.

14 G. He, Y. Lai, Y. Guo, H. Yin, B. Chang, M. Liu, S. Zhang, B. Yang and J. Wang, Tipping Gold Nanobipyramids with Titania for the Use of Plasmonic Hotspots to Drive Amine Coupling, *ACS Appl. Mater. Interfaces*, 2022, **14**(48), 53724–53735, DOI: 10.1021/acsami.2c14554.

15 S. J. Lee, Z. Ku, A. Barve, J. Montoya, W.-Y. Jang, S. R. J. Brueck, M. Sundaram, A. Reisinger, S. Krishna and S. K. Noh, A Monolithically Integrated Plasmonic Infrared Quantum Dot Camera, *Nat. Commun.*, 2011, **2**(1), 286.

16 Y. Karimi, H. Kaatuzian, A. Tooghi and M. Danaie, All-Optical Plasmonic Switches Based on Fano Resonance in an X-Shaped Resonator Coupled to Parallel Stubs for Telecommunication Applications, *Optik*, 2021, **243**, 167424.

17 D. Château, S. David, G. Berginc, C. Lopes, F. Chaput, F. Lerouge, A. Désert, C. Andraud and S. Parola, Plasmonic Bipyramidal Au Nanoparticles Enhance Near-Infrared Nonlinear Absorption of Dyes Confined in Sol–Gel Materials: Implications for the Safe Utilization of Lasers, *ACS Appl. Nano Mater.*, 2022, **5**(3), 3773–3780, DOI: 10.1021/acsanm.1c04422.

18 S. Zhang, K. Bao, N. J. Halas, H. Xu and P. Nordlander, Substrate-Induced Fano Resonances of a Plasmonic Nanocube: A Route to Increased-Sensitivity Localized Surface Plasmon Resonance Sensors Revealed, *Nano Lett.*, 2011, **11**(4), 1657–1663, DOI: 10.1021/nl200135r.

19 M. J. Guffey, R. L. Miller, S. K. Gray and N. F. Scherer, Plasmon-Driven Selective Deposition of Au Bipyramidal Nanoparticles, *Nano Lett.*, 2011, **11**(10), 4058–4066, DOI: 10.1021/nl201020g.

20 G. Weng, X. Shen, J. Li, J. Zhu, J. Yang and J. Zhao, Multipole Plasmon Resonance in Gold Nanobipyramid: Effects of Tip Shape and Size, *Phys. Lett. A*, 2021, **412**, 127577.

21 C. N. Vu, Z. Ouzit, C. Lethiec, M. Pellarin, A. Maitre, F. Lerouge, L. Coolen and J. Laverdant, Polarimetric Dark-Field Spectroscopy of Gold Bipyramids: Measuring Single Particle 3D Orientation, *Opt. Commun.*, 2022, **510**, 127947.

22 A. Khitous, C. Molinaro, S. Abdallah, J.-P. Malval, S. Marguet and O. Soppera, *Experimental Observation of Thermoplasmonic Heat Transfer at the Nanoscale by Polymerization. A Step towards Nanoscale Heat Sources*, 2024.

23 F. Kameche, W. Heni, S. Telitel, D. Ge, L. Vidal, F. Dumur, D. Gigmes, J. Lalevee, S. Marguet and L. Douillard, Plasmon-Triggered Living Photopolymerization for Elaboration of Hybrid Polymer/Metal Nanoparticles, *Mater. Today*, 2020, **40**, 38–47.

24 Y. Wang, S. Wang, S. Zhang, O. A. Scherman, J. J. Baumberg, T. Ding and H. Xu, Plasmon-Directed Polymerization: Regulating Polymer Growth with Light, *Nano Res.*, 2018, **11**(12), 6384–6390, DOI: 10.1007/s12274-018-2163-0.

25 J. Waxenegger, A. Trügler and U. Hohenester, Plasmonics Simulations with the MNPBEM Toolbox: Consideration of Substrates and Layer Structures, *Comput. Phys. Commun.*, 2015, **193**, 138–150.

26 U. Hohenester and A. Trügler, MNPBEM–A Matlab Toolbox for the Simulation of Plasmonic Nanoparticles, *Comput. Phys. Commun.*, 2012, **183**(2), 370–381.

27 D. Chateau, A. Liotta, F. Vadcard, J. R. G. Navarro, F. Chaput, J. Lermé, F. Lerouge and S. Parola, From gold nanobipyramids to nanojavelins for a precise tuning of the Plasmon resonance to the infrared wavelengths. Experimental and theoretical aspects, *Nanoscale*, 2015, **7**, 1934–1943, DOI: 10.1039/C4NR06323F.

28 P. B. Johnson and R. W. Christy, Optical Constants of the Noble Metals, *Phys. Rev. B: Solid State*, 1972, **6**(12), 4370–4379, DOI: 10.1103/PhysRevB.6.4370.

29 C. Vu, Z. Ouzit, C. Lethiec, A. Maitre, L. Coolen, F. Lerouge, M. Pellarin and J. Laverdant, 3D Orientation of Single Gold Bipyramid Measured by Scattering Polarization Pectroscopy: Role of the Numerical Aperture, *Sens. Transducers J.*, 2022, **255**(1), 10.

30 C. Deeb, C. Ecoffet, R. Bachelot, J. Plain, A. Bouhelier and O. Soppera, Plasmon-Based Free-Radical Photopolymerization: Effect of Diffusion on Nanolithography Processes, *J. Am. Chem. Soc.*, 2011, **133**(27), 10535–10542.

31 A. Khitous, L. Lartigue, J. Moreau and O. Soppera, Insights into Photopolymerization at the Nanoscale Using Surface Plasmon Resonance Imaging, *Small*, 2024, **240**, 1885, DOI: 10.1002/smll.202401885.